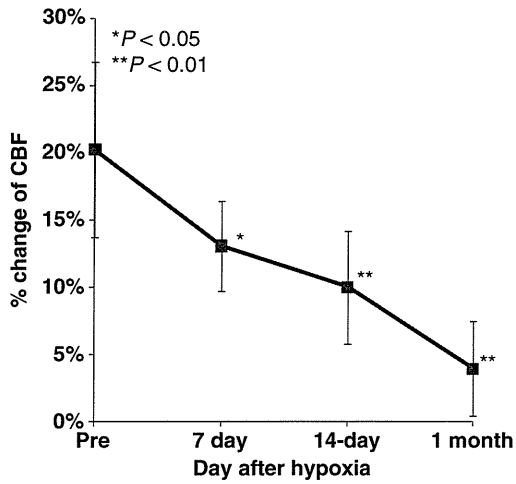

Figure 3. Longitudinal cerebral blood flow (*CBF*) measurements under chronic hypoxia. Increase in *CBF* response to sensory stimulation was consistently observed at pre, 7 days, 14 days, and 1 month. Bold squares and line represent the mean of all animal data of average values at each measurement day. Error bars indicate s.d. $*P<0.05$, $**P<0.01$.

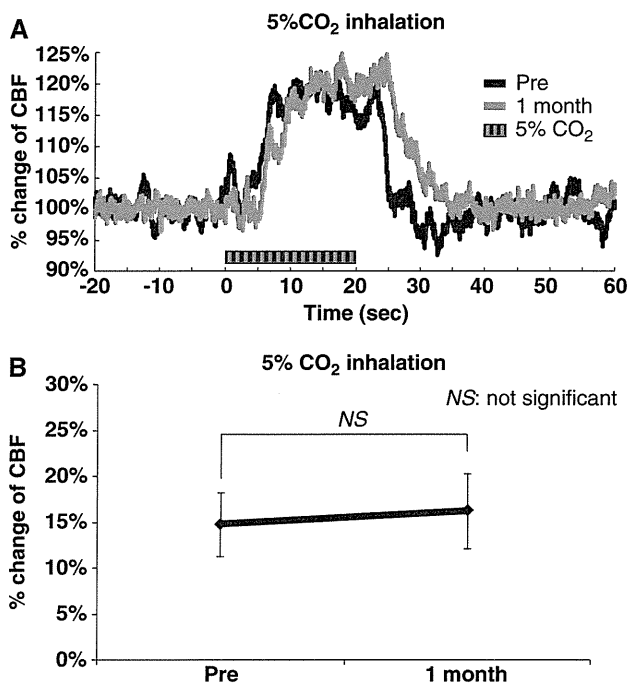

Figure 4. Increase in cerebral blood flow (*CBF*) evoked by 5% CO_2 inhalation. (**A**) Time–response curve of increase in *CBF*. Time–response curves were normalized to the baseline level (20 seconds before sensory stimulation) and shown for one representative animal. Horizontal bars indicate the stimulation period. (**B**) Mean percentage increase in *CBF* within 10 to 20 seconds 5% CO_2 inhalation ($N=5$). Error bars indicate s.d.

Neural Response to Whisker Stimulation

Figure 5 shows the representative fluorescent VSD signals evoked by a single sensory stimulation after 1 month of chronic hypoxia (Figure 5). The region of neuronal activity before chronic hypoxia was almost identical to that after 1 month of hypoxia (Figure 5A). There were no significant differences in the number of pixels between before and after 1 month of chronic hypoxia (Figure 5B).

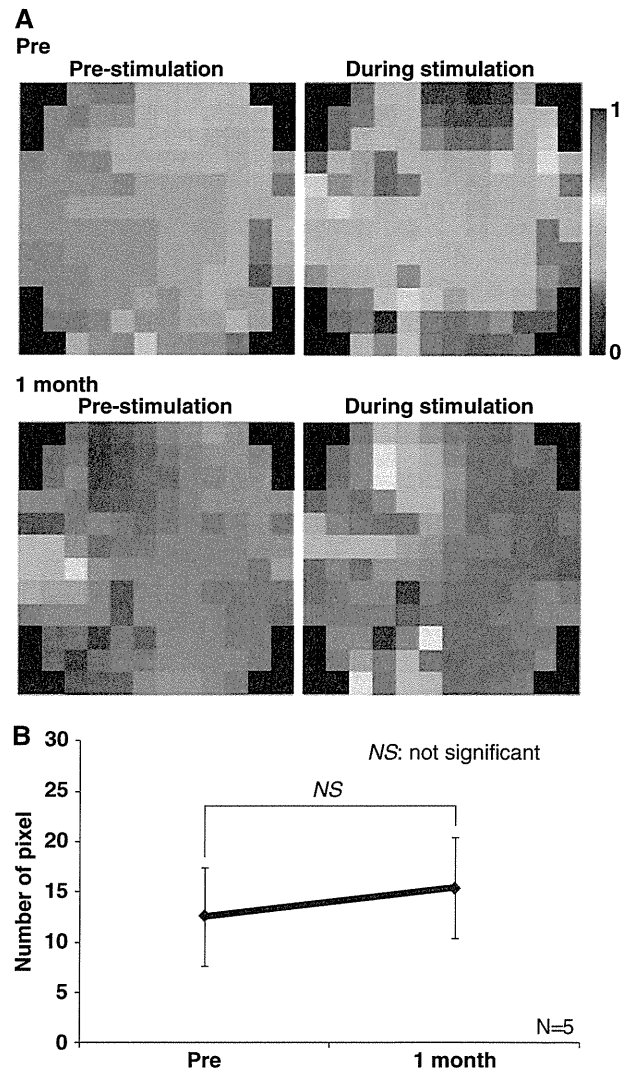

Figure 5. Neuronal activities evoked by sensory stimulation under chronic hypoxia condition. (**A**) Activation maps of voltage-sensitive dye (VSD) imaging experiment performed before (top) and 1 month (bottom) after chronic hypoxia, shown for one representative animal. Right and left frames showed VSD imagings before and immediately after sensory stimulation, respectively. (**B**) Summary of VSD results in five animals. There was no significant difference in the number of pixels between pre and 1 month.

Effects of Changes in Effective Diffusivity for Oxygen in the Capillary Bed (D) by Chronic Hypoxia

The relation between changes in *CBF* and $CMRO_2$, corresponding to *CBF* multiplied by *OEF*, during neural activation for each *D* value was simulated using Hyder's model[19] as shown in Figure 6. Based on the simulation results in Figure 6, a 690% increase in *CBF* during neuronal activation is required for a 10% increase in $CMRO_2$ when *D* remained at 0.223 in spite of chronic hypoxia. As mention above, the *D* values increased from 0.223 to 0.466 to 0.669 after 3 weeks of chronic hypoxia as a result of a 96% to 189% increase in capillary blood volume.[7] The results shown in Figure 5 indicated that neuronal activation at somatosensory cortex was quite stable throughout the 1 month of chronic hypoxia, indicating that $CMRO_2$ was also stable. Thus, as a result of the increase in *D* (0.466 to 0.669) caused by chronic hypoxia, no increase in *CBF* is required for the 10% increase in $CMRO_2$ (Figure 6) because, in the case of $D=0.466$ to 0.669, the % change in $CMRO_2$ was already above 10%, even if *CBF* did not increase.

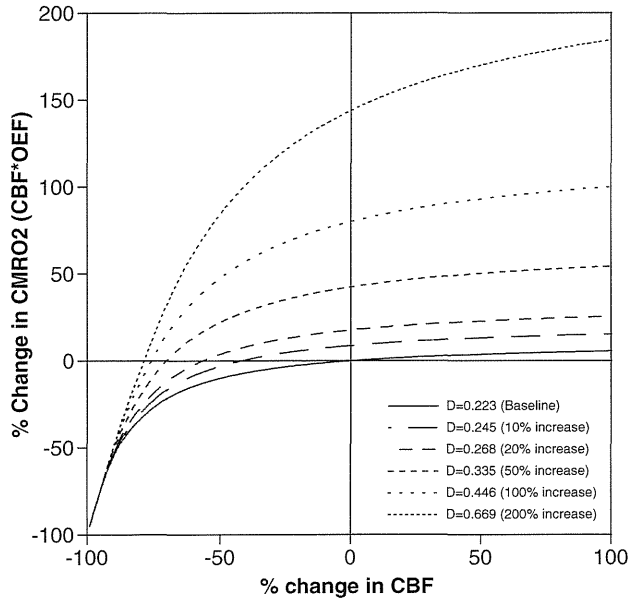

Figure 6. Simulation result of Hyder's model. Solid and dashed lines indicated the relationship between cerebral metabolic rate of oxygen utilization ($CMRO_2$) and cerebral blood flow (CBF) among the respective D values.

DISCUSSION

We performed *LDF* measurements in awake mice maintained under chronic hypoxic conditions. Although adaptation of the baseline *CBF* to chronic hypoxia has been previously investigated using human and animal models, this study represents the first observation of the effects of chronic hypoxia on the hemodynamic responses in awake mice. In this work, we observed that chronic hypoxia causes a significant reduction of the increase in *CBF* evoked by sensory stimulation. Previous study using BOLD fMRI (blood oxygen level-dependent functional magnetic resonance imaging) showed reduced cerebrovascular response to visual stimulation in native-born high-altitude residents as compared with native-born sea-level residents.[20] These results might be related to our results of changes in *CBF* during neural activation.

The reduction in the increase of *CBF* during neuronal activation appeared to lead to a reduction in the increase of the oxygen supply to the brain. To explain the reasons for the reduction of the increase in *CBF* during stimulation under chronic hypoxic conditions, we hypothesized that this reduction was caused by (1) cerebrovascular dysfunction, (2) neuronal dysfunction, and (3) regulation of hemodynamics to adapt to the chronic hypoxic condition. Because the hypercapnic *CBF* response was not reduced, vascular dilatory function was sufficiently sustained in the chronic hypoxia mice. Moreover, VSD imaging showed no attenuation of neuronal activation during sensory stimulation during the 1 month of chronic hypoxia. Based on these findings, it was clear that the reduction in the increase in functional hyperemia under chronic hypoxic conditions was not caused either by cerebrovascular dysfunction or by neuronal dysfunction in the somatosensory cortex.

As mentioned above, we have previously reported that the vasodilation induced by chronic hypoxia occurred mainly in the parenchymal capillaries, indicating the ability to adjust the diameter in response to the oxygen environment.[7] Based on Hyder's model,[19] the relation between changes in *CBF* and $CMRO_2$, corresponding to *CBF* multiplied by *OEF*, during neural activation can be simulated for each D value, which is in proportion to capillary blood volume, as shown in Figure 6. This simulation study shows that when D increases by chronic hypoxia, an increase in $CMRO_2$ during neural activation can be revealed without any increase in *CBF*. On the other hand, the oxygen content (C_a) of mice might be changed during hypoxic condition. C_a is expressed as follows:

$$C_a = \alpha \times Hb \times SaO_2 + \beta \times PaO_2,$$

where α is the oxygen binding capacity of hemoglobin (1.39 mL/g),[21] *Hb* is the hemoglobin concentration (g/dL), SaO_2 is arterial O_2 saturation, PaO_2 is arterial oxygen partial pressure (mm Hg), and β is the oxygen solubility (0.00315 mL per 100 mL per mm Hg). When the hypoxic condition (8% O_2) decreased PaO_2 from 100 to 40 mm Hg, SaO_2 was decreased from 0.92 to 0.47 (P_{50} of mouse = 41.5 mm Hg; pH = 7.40).[22] The hematocrit results in our study indicated that hemoglobin was increased by about two times during chronic hypoxia. Based on these parameters, C_a remained almost unchanged under hypoxia (19.73 mL/mL blood) as compared with that under normoxia (19.50 mL/mL blood).

The adaptive regulation mechanism of *CBF* responses during chronic hypoxia must be associated with several factors. One possibility is the inhibition of a synthetase of a vasoactive mediator (e.g., nitric oxide, cyclooxygenase-2, and adenosine) released from neurons and glia by neural activity[23–25] or by disturbing astrocyte function, which is associated with neurovascular coupling.[26] Especially, nitric oxide is associated with hypoxia-inducible factor-1 activity,[27,28] suggesting that nitric oxide plays an important role in the cerebrovascular tone in chronic hypoxia and might also affect to the reduction of increase in *CBF*. To explore the mechanism, further experiments using synthetase inhibitors or immunostaining techniques in mice need to be performed.

Using positron emission tomography in human subjects, Mintun *et al*[10] has shown that hemodynamic response to visual stimulation was identical between normoxia and mild acute hypoxia (fraction of inspired oxygen; FiO_2 of 12%) conditions.[11] These findings suggest that the neural activity-induced *CBF* response is determined by factors other than local requirements of oxygen. On the other hand, in the present study, the long-term low oxygen condition could be modified by neurovascular coupling, and the simulation results suggested that the reduction in the increase in *CBF* contributed to the balance between oxygen supply and metabolism in the brain. In other words, the hemodynamic response to neuronal activation can be modified in response to the change in their balance to energy demand. The discrepancy between acute hypoxia and chronic hypoxia could be explained as follows. A short-term exposure to hypoxia may not produce a stabilized baseline state, whereas a long-term exposure produces a newly established baseline state in which the oxygen supply-demand level can be balanced. Further experiments are needed to elucidate this slow adaptation mechanism of neurovascular coupling to changes in the oxygen environment, which involve (1) sensing the tissue oxygen state, (2) monitoring the supply-demand balance, and (3) controlling the magnification factor of *CBF* changes in neurovascular coupling.

In summary, we found a reduction in the increase in *CBF* evoked by neuronal activation in mice occurring during 1 month of chronic hypoxia. The results of the simulation using Hyder's model indicated that a slight increase in *CBF* caused a large increase in oxygen supply to the brain under increased D value conditions. The adaptation mechanisms underlying the reduction in the increase of *CBF* under chronic hypoxia remain to be identified. To explore these mechanisms, further experiments using synthetase inhibitors or immunostaining techniques on mice should be performed.

DISCLOSURE/CONFLICT OF INTEREST

The authors declare no conflict of interest.

REFERENCES

1 LaManna JC, Chavez JC, Pichiule P. Structural and functional adaptation to hypoxia in the rat brain. *J Exp Biol* 2004; **207**: 3163–3169.
2 Ainslie PN, Ogoh S. Regulation of cerebral blood flow in mammals during chronic hypoxia: a matter of balance. *Exp Physiol* 2010; **95**: 251–262.
3 Wilson M, Newman HS, Imray C. The cerebral effects of ascent to high altitudes. *Lancet Neurol* 2009; **8**: 175–191.
4 Jensen JB, Sperling B, Severinghaus JW, Lassen NA. Augmented hypoxic cerebral vasodilation in men during 5 days at 3,810 m altitude. *J Appl Physiol* 1996; **80**: 1214–1218.
5 Pichiule P, LaManna JC. Angiopoietin-2 and rat brain capillary remodeling during adaptation and deadaptation to prolonged mild hypoxia. *J Appl Physiol* 2002; **93**: 1131–1139.
6 Boero JA, Ascher J, Arregui A, Rovainen C, Woolsey TA. Increased brain capillaries in chronic hypoxia. *J Appl Physiol* 1999; **86**: 1211–1219.
7 Yoshihara K, Takuwa H, Kanno I, Okawa S, Yamada Y, Masamoto K. 3D analysis of intracortical microvasculature during chronic hypoxia in mouse brains. *Adv Exp Med Biol* 2013; **765**: 357–363.
8 Xu K, Lamanna JC. Chronic hypoxia and the cerebral circulation. *J Appl Physiol* 2006; **100**: 725–730.
9 Ndubuizu OI, Tsipis CP, Li A, LaManna JC. Hypoxia-inducible factor-1 (HIF-1)-independent microvascular angiogenesis in the aged rat brain. *Brain Res* 2010; **1366**: 101–109.
10 Mintun MA, Lundstrom BN, Snyder AZ, Vlassenko AG, Shulman GL, Raichle ME. Blood flow and oxygen delivery to human brain during functional activity: theoretical modeling and experimental data. *Proc Natl Acad Sci USA* 2001; **98**: 6859–6864.
11 Lindauer U, Gethmann J, Kühl M, Kohl-Bareis M, Dirnagl U. Neuronal activity-induced changes of local cerebral microvascular blood oxygenation in the rat: effect of systemic hyperoxia or hypoxia. *Brain Res* 2003; **975**: 135–140.
12 Sicard KM, Duong TQ. Effects of hypoxia, hyperoxia, and hypercapnia on baseline and stimulus-evoked BOLD, CBF, and CMRO2 in spontaneously breathing animals. *Neuroimage* 2005; **25**: 850–858.
13 Takuwa H, Matsuura T, Bakalova R, Obata T, Kanno I. Contribution of nitric oxide to cerebral blood flow regulation under hypoxia in rats. *J Physiol Sci* 2010; **60**: 399–406.
14 Tomita Y, Kubis N, Calando Y, Tran Dinh A, Meric P, Seylaz J *et al.* Long-term in vivo investigation of mouse cerebral microcirculation by fluorescence confocal microscopy in the area of focal ischemia. *J Cereb Blood Flow Metab* 2005; **25**: 858–867.
15 Yoshida T, Sakagami M, Katura T, Yamazaki K, Tanaka S, Iwamoto M *et al.* Anisotropic spatial coherence of ongoing and spontaneous activities in auditory cortex. *Neurosci Res* 2008; **61**: 49–55.
16 Takuwa H, Autio J, Nakayama H, Matsuura T, Obata T, Okada E *et al.* Reproducibility and variance of a stimulation-induced hemodynamic response in barrel cortex of awake behaving mice. *Brain Res* 2011; **1369**: 103–111.
17 Limbourg FP, Huang Z, Plumier JC, Simoncini T, Fujioka M, Tuckermann J *et al.* Rapid nontranscriptional activation of endothelial nitric oxide synthase mediates increased cerebral blood flow and stroke protection by corticosteroids. *J Clin Invest* 2002; **110**: 1729–1738.
18 Mizuma H, Shukuri M, Hayashi T, Watanabe Y, Onoe H. Establishment of in vivo brain imaging method in conscious mice. *J Nucl Med* 2010; **51**: 1068–1075.
19 Hyder F, Shulman RG, Rothman DL. A model for the regulation of cerebral oxygen delivery. *J Appl Physiol* 1998; **85**: 554–564.
20 Yan X, Zhang J, Gong Q, Weng X. Cerebrovascular reactivity among native-raised high altitude residents: an fMRI study. *BMC Neurosci* 2011; **12**: 94–104.
21 International Committee for Standardization in Haematology. Recommendations for haemoglobinometry in human blood. *Br J Haemat* 1967; **13**(Suppl): 71–75.
22 Gray LH, Steadman JM. Determination of the oxyhaemoglobin dissociation curves for mouse and rat blood. *J Physiol* 1964; **175**: 161–171.
23 Yang G, Zhang Y, Ross ME, Iadecola C. Attenuation of activity-induced increases in cerebellar blood flow in mice lacking neuronal nitric oxide synthase. *Am J Physiol Heart Circ Physiol* 2003; **285**: 298–304.
24 Bakalova R, Matsuura T, Kanno I. The cyclooxygenase inhibitors indomethacin and rofecoxib reduce regional cerebral blood flow evoked by somatosensory stimulation in rats. *Exp Biol Med* 2002; **227**: 465–473.
25 Ko KR, Ngai AC, Winn RH. Role of adenosine in regulation of regional cerebral blood flow in sensory cortex. *Am J Physiol* 1990; **259**: 1703–1708.
26 Attwell D, Buchan AM, Charpak S, Lauritzen M, Macvicar BA, Newman EA. Glial and neuronal control of brain blood flow. *Nature* 2010; **468**: 232–243.
27 Agani FH, Puchowicz M, Chavez JC, Pichiule P, LaManna J. Role of nitric oxide in the regulation of HIF-1alpha expression during hypoxia. *Am J Physiol Cell Physiol* 2002; **283**: 178–186.
28 Cattaneo MG, Cappellini E, Benfante R, Ragni M, Omodeo-Salè F, Nisoli E *et al.* Chronic deficiency of nitric oxide affects hypoxia inducible factor-1α (HIF-1α) stability and migration in human endothelial cells. *PLoS One* 2011; **6**: e29680.

Journal of Neuroscience Research

Journal of Neuroscience Research 91:578–584 (2013)

Potassium-Induced Cortical Spreading Depression Bilaterally Suppresses the Electroencephalogram but Only Ipsilaterally Affects Red Blood Cell Velocity in Intraparenchymal Capillaries

Miyuki Unekawa,[1]* Yutaka Tomita,[1] Haruki Toriumi,[1] Kazuto Masamoto,[2,3] Iwao Kanno,[3] and Norihiro Suzuki[1]

[1]Department of Neurology, School of Medicine, Keio University, Tokyo, Japan
[2]Center for Frontier Science and Engineering, University of Electro-Communications, Tokyo, Japan
[3]Molecular Imaging Center, National Institute of Radiological Sciences, Chiba, Japan

Cortical spreading depression (CSD) is a repetitive, propagating profile of mass depolarization of neuronal and glial cells, followed by sustained suppression of spontaneous neuronal activity. We have reported a long-lasting suppressive effect on red blood cell (RBC) velocities in intraparenchymal capillaries. Here, to test the hypothesis that the prolonged decrease of RBC velocity in capillaries is due to suppression of neuronal activity, we measured CSD-elicited changes in the electroencephalogram (EEG) as an index of neuronal activity. In isoflurane-anesthetized rats, DC potential, EEG, partial pressure of oxygen (PO_2), and cerebral blood flow (CBF) were simultaneously recorded in the temporo-parietal region. The velocities of fluorescently labeled RBCs were evaluated by high-speed camera laser scanning confocal fluorescence microscopy with our original software, KEIO-IS2. Transient deflection of DC potential and PO_2 and increase of CBF were repeatedly detected only in the ipsilateral hemisphere following topical KCl application. On the other hand, the relative spectral power of EEG was reduced bilaterally, showing the lowest value at 5 min after KCl application, when the other parameters had already returned to the baseline after the passage of CSD. Mean RBC velocity in capillaries was slightly but significantly reduced during and after passage of CSD in the ipsilateral hemisphere but did not change in the contralateral hemisphere in the same rats. We suggest that mass depolarization of neuronal and glial cells might transiently decelerate RBCs in nearby capillaries, but the sustained reduction of ipsilateral RBC velocity might be a result of the prolonged effect of CSD, not of neuronal suppression alone.

Key words: cortical spreading depression; cerebral microcirculation; electroencephalogram; transhemispheric projection; RBC velocity

Cortical spreading depression (CSD) is a repetitive mass depolarization of neuronal and glial cells, followed by a sustained suppression of spontaneous neuronal activity (Leão, 1944). CSD is involved in the mechanism of migraine aura, which starts in the primary visual cortex and moves toward the periphery at the rate of approximately 3 mm/min (Lauritzen, 2001). At the beginning of migraine attacks, cerebral blood flow (CBF) decreases in the posterior part of the brain, and then the hypoperfusion spreads into the parietal and temporal lobes at the rate of 2–3 mm/min for 30–60 min (so-called spreading oligemia; Olesen et al., 1981). In an experimental model, artificially evoked CSD elicited a rise of CBF, followed by a long-lasting reduction to below the prestimulus level (Lauritzen et al., 1982; Kocher, 1990; Fabricius and Lauritzen, 1993).

It has been accepted that CSD does not propagate from one hemisphere to the other and does not interfere with the circulation or cause edema in the contralateral cortex (Bueš et al., 1974). The side of the headache usually corresponds to the side of the vascular changes (Olesen et al., 1990). On the other hand, CSD induced by fine-needle stab or topical application of tetrodotoxin (TTX) elicited a pronounced decrease of the spontaneous spike rate in layers III through IV of the contralateral cortex (Enager et al., 2004). Electrical stimulation of transcallosal fibers produces electrophysiologic and

Contract grant sponsor: Ministry of Education, Culture, Sports, Science and Technology of Japan; Contract grant number: 22390182 (to N.S.); Contract grant number: 24500422 (to Y.T.); Contract grant sponsor: Otsuka Pharmaceutical Co., Ltd.

*Correspondence to: Miyuki Unekawa, Department of Neurology, School of Medicine, Keio University, 35 Shinanomachi, Shinjuku-ku, Tokyo 160-8582, Japan. E-mail: unekawa.m@z5.keio.jp

Received 27 June 2012; Revised 10 October 2012; Accepted 10 November 2012

Published online 18 January 2013 in Wiley Online Library (wileyonlinelibrary.com). DOI: 10.1002/jnr.23184

hemodynamic responses in contralateral cortical regions via neuronal transmission (Hoffmeyer et al., 2007). Furthermore, stimulation of the hindpaw motor cortex evoked a bilateral blood oxygenation level-dependent fMRI signal via corticocortical pathways (Austin et al., 2003). Mono- and polysynaptic connections, including callosal cells, are involved in interhemisphere interactions (Bogdanova and Sil'kis, 1999). Thus, it is likely that unilateral elicitation of CSD would affect neuronal activity in the contralateral hemisphere.

Recently, the concept of the neurovascular unit, in which neurons and microvessels appear to communicate with each other, with the participation of the intervening astrocytes, has been proposed and investigated (del Zoppo, 2010). Namely, neuronal activity and microcirculation in the adjacent area are closely interlinked. Red blood cell (RBC) behavior in capillaries is especially important, because RBCs are the predominant oxygen carrier from the lung to the tissue. We have found that RBC velocity in intraparenchymal capillaries is often independent of upstream arteriolar blood flow or tissue perfusion in the surrounding microvasculature; for example, RBC velocity in capillaries remained unchanged in response to topical application of nitroprusside on the brain surface in spite of a dramatic increase in local CBF (Tomita et al., 2009).

We have developed a method for measurement of the velocity of individual RBCs in capillaries *in vivo*, using a high-speed camera laser scanning confocal fluorescence microscope system with Matlab-domain analysis software, KEIO-IS2 (Schiszler et al., 2005; Tomita et al., 2008; Unekawa et al., 2008). We observed heterogeneous changes of RBC velocity in capillaries, namely, both a sustained decrease and a remarkable increase, after KCl application on the cerebral cortex, while CBF as measured by laser Doppler flowmetry was elevated (Unekawa et al., 2012). In that study, the number of slowed RBCs was dramatically increased during CSD, and a similar tendency was seen even after passage of CSD, in spite of the recovery of DC potential, partial pressure of oxygen (PO_2), and CBF.

In the course of our study, we noticed that the electroencephalogram (EEG), reflecting spontaneous neuronal activity was bilaterally suppressed even after the passage of CSD. We speculated that the prolonged decrease of RBC velocity was due to this suppression of neuronal activity. To examine this hypothesis, we simultaneously evaluated the transhemispheric effects on spontaneous neuronal activity and on RBC velocity in intraparencymal capillaries in response to potassium-induced CSD in the same animal. We discuss the relationship between neuronal activity and RBC flow in single capillaries.

MATERIALS AND METHODS

General Procedures

Animals were used with the approval (No. 09058) of the Animal Ethics Committee of Keio University (Tokyo, Japan), and all experimental procedures were in accordance with the university's guidelines for the care and use of laboratory animals. General procedures were as described in our previous article (Unekawa et al., 2012). Male Sprague-Dawley rats (CLEA Japan, Inc., Tokyo, Japan; 10–15 weeks, body weight 411 ± 134 g, n = 17) were anesthetized with isoflurane (2.5–3.0% in room air, with a flow rate of 250 ml/min) via a concentration-controllable anesthesia unit (model 400; Univentor Ltd., Zejtun, Malta). Arterial blood pressure (ABP) was continuously recorded through a femoral arterial catheter via a surgical strain-gauge (MLT0670 and ML117; ADInstruments Pty. Ltd., Bella Vista, New South Wales, Australia), and heart rate (HR) was determined from the ABP wave. Body temperature was maintained with a heating pad and thermocontroller (BWT-100; Bioresearch Center Co., Ltd., Nagoya, Japan).

Study of Transhemispheric Effects

Measurements of PO_2, CBF, and DC potential were made as described in our previous article (Unekawa et al., 2012). Each rat was fixed to a head-holder (SG-3N, modified to be flexible around the horizontal axis; Narishige Scientific Instrument Laboratory, Tokyo, Japan), and two windows of approximately 3 mm width were made bilaterally at the parieto-temporal region of the cerebral cortex. As shown in Figure 1A,B (n = 7), an electrode for measuring PO_2 (POE-10N; Bioresearch Center Co., Ltd.), an electrode for DC potential (EEG-5002Ag; Bioresearch Center Co., Ltd.), and the probe of a laser Doppler flowmeter (ALF 21R; Advance Co., Ltd., Tokyo, Japan) were positioned at the right window, and another electrode for DC potential was positioned at the left window, after removal of the dura. These electrodes and probe were fixed in place and sealed with dental cement to prevent the brain surface from drying. Reference electrodes for PO_2 (POR-10N; Bioresearch Center Co., Ltd.) and DC potential (EER-5004Ag; Bioresearch Center Co., Ltd.) were placed subcutaneously in the back and under the scalp, respectively. PO_2 was continuously monitored with an oxygen monitor (PO2-100DW; Inter Medical Co., Ltd., Nagoya, Japan). The DC potential was amplified at 1–100 Hz with a sampling rate of 1 kHz using a differential headstage and a differential extracellular amplifier (models 4002 and EX1; Dagan Co., Minneapolis, MN). Continuous recordings of ABP as well as HR, PO_2, CBF, and DC potential were stored on a multichannel recorder (PowerLab 8/30; ADInstruments Pty Ltd.) and evaluated with off-line analysis software (LabChart; ADInstruments Pty Ltd.). EEG was obtained by digital filtering of the DC potential signal with a 5-Hz low cut, to minimize basal fluctuations resulting from heart rate and breathing. The EEG signal was calculated by fast Fourier frequency analysis every 1 min, and the maximum value at each frequency was employed to determine EEG spectral power. The peak value was found at the frequency of about 8–11 Hz, namely, α-wave, in all rats. PO_2, CBF, and DC potential were averaged for every 10 sec. KCl solution (1.0 M, 5 μl) was applied into a posterior hole on either side having a center at the coordinates of 7 mm posterior and 2 mm lateral to bregma, after confirmation that all parameters had remained stable for at least 10 min, and a further application was made into the

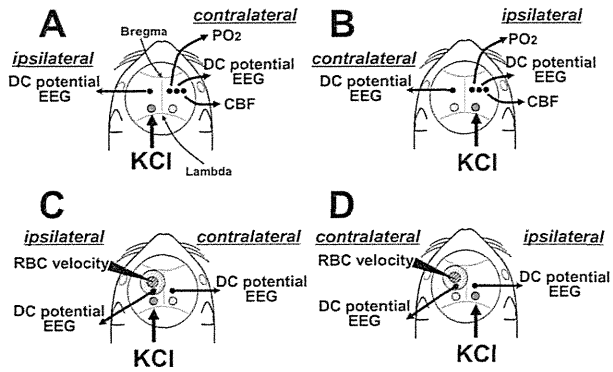

Fig. 1. Positioning of electrodes for DC potential, an electrode for PO_2, and a laser Doppler flowmeter probe in the cranial window for transhemispheric study (**A,B**) and RBC velocity study (**C,D**). EEG was calculated from the DC potential signal as mentioned in Materials and Methods. When KCl was applied to the left hole, contralateral DC potential, PO_2, and CBF were recorded in parallel with ipsilateral DC potential (A). When KCl was applied to the right hole, ipsilateral DC potential, PO_2, and CBF were recorded in parallel with contralateral DC potential (B) in the same rat. Ipsilateral or contralateral confocal movies were obtained in the shaded area to measure RBC velocity before and after application of KCl to the left (C) or the right (D) hole, respectively.

posterior hole on the other side at least 30 min after the last CSD, when all parameters including EEG had recovered. KCl application at the concentration used here elicited several CSD episodes within a 20-min interval without exception, but analysis of EEG and other parameters was performed during the first CSD episode to avoid the influence of the previous episode(s).

Analysis of RBC Velocity

Measurement of RBC velocity was conducted as described previously (Tomita et al., 2008; Unekawa et al., 2008). A cranial window of approximately 4 mm diameter was made at the left parietotemporal region of the cerebral cortex. As shown in Figure 1C,D (n = 10), DC potential electrodes were fixed at the posterior edge of the left window and at the symmetric position across the sagittal suture on the contralateral side. KCl solution (1.0 M, 5 μl) was applied alternately into the additional posterior holes on both sides, having a center at the coordinates of 7 mm posterior and 2 mm lateral to bregma. An appropriate capillary-rich area around the center of the cranial window was selected, and 0.5 ml of fluorescein isothiocyanate (FITC)-labeled RBC suspension, prepared beforehand according to Seylaz et al. (1999), was injected into the bloodstream so that the final percentage of FITC-labeled RBCs/total RBCs in the circulating blood was approximately 0.4%. The velocities of individual FITC-labeled RBCs were automatically calculated using a high-speed camera (500 fps) laser scanning confocal fluorescence microscope and an image analysis system in the Matlab (The MathWorks, Natick, MA) environment with application software (KEIO-IS2) developed in our laboratory (Schiszler et al., 2005; Tomita et al., 2008). Motion images were obtained at the depth of approximately 80 μm from the brain surface (layer I of the cerebral cortex) and analyzed in an area of 600 × 400 μm. The images acquired with the high-speed system could be recorded for up to 15 sec because of the limitation of file size (2 GB) in our analysis system. With reference to alternatively recorded images obtained using a conventional video camera, we defined single capillaries as having a diameter of less than 10 μm, based on other reports (Williams et al., 1993; Hutchinson et al., 2006). The frequency distribution of RBC velocity was obtained by classification of velocities in steps of 0.5 mm/sec and counting the RBCs within each step. RBC appearance was represented as a percentage of the total number of detected RBCs.

Statistical Analysis

All data are reported as mean ± SD. Statistical analysis of transhemispheric effects was performed via Student's *t*-test after Levene's test for equality of variance. Statistical analysis of EEG spectral power was performed with paired parametric multiple comparison (Bonferroni's test) after demonstration of homogeneity with repeated-measures ANOVA (Friedman's test). Statistical analysis of frequency distribution of RBC velocity was performed with nonparametric multiple comparisons (Bonferroni's test) after demonstration of homogeneity of variance with one-way ANOVA (Kruskal Wallis test). $P < 0.05$ was considered statistically significant.

RESULTS

General Results

Initial levels of mean ABP (MABP) and HR were 75 ± 6 mmHg and 327 ± 49 bpm, respectively. MABP and HR were maintained within ±20 mmHg and ±50 bpm in each rat throughout the experiments. MABP did not decrease below 60 mmHg in any rat. Average MABP and HR were 72 ± 12 mmHg and 314 ± 51 bpm at the end of the experiment.

Transhemispheric Effect of CSD

When KCl was applied to the left side, as shown in Figure 1A, DC potential, PO_2, and CBF of the right (contralateral) side did not change, whereas DC potential deflection was seen on the left (ipsilateral) side (Fig. 2A). In the same rat, when KCl was applied to the right side, as shown in Figure 1B, DC potential, PO_2, and CBF on the right (ipsilateral) side showed a specific response as described previously (Unekawa et al., 2012), without DC potential deflection at the left (contralateral) side, as shown in Figure 2B. Namely, potassium-induced responses of DC potential, PO_2, and CBF propagated only within the same hemisphere. On the other hand, EEG was bilaterally suppressed for a longer time. ABP was constant independently of the site of KCl application; that is, the responses were locally elicited and were not due to a change in systemic BP.

Average changes of DC potential, PO_2, CBF, and EEG spectral power on the ipsilateral and contralateral sides after KCl application are plotted in Figure 3. DC potential deflection, transient decrease in PO_2, and

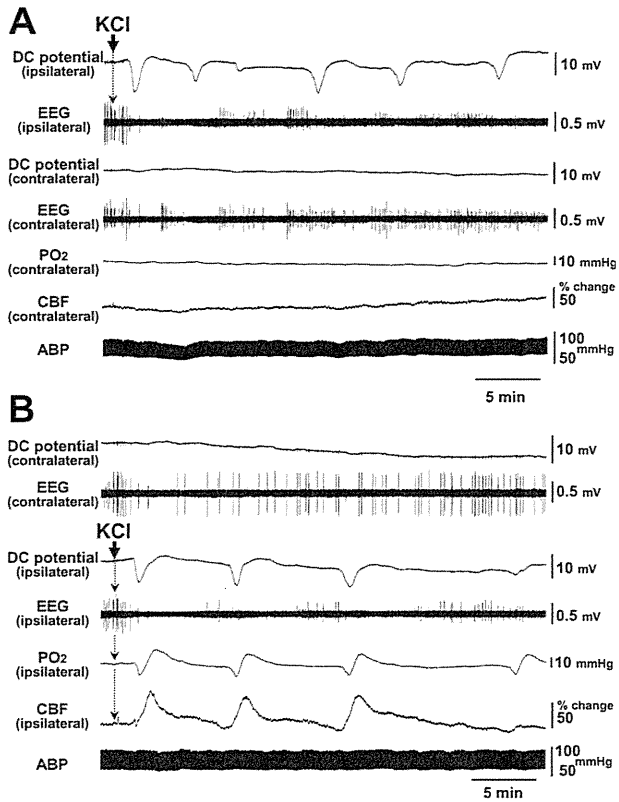

Fig. 2. Sample recordings of DC potential, EEG, PO_2, CBF, and ABP in response to KCl application. **A:** Response to KCl application on the left side, as shown in Figure 1A. **B:** Response to KCl application on the right side, as shown in Figure 1B in the same rat.

increase in CBF were observed on the ipsilateral side (Fig. 3A). However, these parameters did not change at all on the contralateral side (Fig. 3B). On the other hand, EEG spectral power was reduced in a sustained manner on both sides after unilateral application of KCl, showing a trough at 5 min after KCl application, when the other parameters had recovered to their base levels. The suppressive response on the ipsilateral side was statistically significantly larger than that on the contralateral side (Fig. 3C).

Change of RBC Velocity in Capillaries

As shown in Figure 4A, confocal microscopic movies for the analysis of RBC velocity were recorded for 10–15 sec at representative periods, i.e., before KCl application (Before-KCl), just after the trough of the DC potential at the ipsilateral side (Intra-CSD), between CSD when all parameters had returned to the baseline (Inter-CSD), and approximately 1 hr after KCl application when CSD had ceased (After-CSD), in the same manner as in the previous report (Unekawa et al., 2012).

RBC appearance (frequency distribution of RBC velocity in capillaries) showed a peak in the range of 1.0–1.5 mm/sec, with tailing to higher velocities of up to 8.6 mm/sec (Fig. 4B,C; see Before-KCl), which is broadly consistent with our previous findings (Unekawa et al., 2008). After ipsilateral application of KCl, the peak was shifted to the range of 0.5–1.0 mm/sec, namely, to slower velocity (Fig. 4B). This tendency was more apparent at Intra-CSD than at Inter-CSD, again in agreement with our previous report (Unekawa et al., 2012). Mean RBC velocity in single capillaries after ipsilateral application of KCl was statistically significantly decreased to 1.48 ± 1.18 mm/sec (for 337 detected RBCs) at Intra-CSD from the level of Before-KCl (1.74 ± 1.35 mm/sec for 527 detected RBCs), as shown in Figure 4B (inset). The mean velocity was further decreased to 1.34 ± 0.94 mm/sec (for 291 detected RBCs) at Inter-CSD and 1.31 ± 0.72 mm/sec (for 239 detected RBCs) at After-CSD. On the other hand, contralateral application of KCl did not affect the frequency distribution at any recording period (Fig. 4C). The mean velocity after contralateral application of KCl in the same rat was unchanged throughout the serial recording period (Before-KCl, 1.72 ± 1.05 mm/sec for 1,047 detected RBCs; Intra-CSD, 1.68 ± 1.11 mm/sec for 1,406 detected RBCs; Inter-CSD, 1.72 ± 1.14 mm/s for 1,005 detected RBCs; After-CSD, 1.68 ± 1.34 mm/sec for 593 detected RBCs), as shown in Figure 4C (inset).

DISCUSSION

The occurrence of propagating unilateral CSD within the ipsilateral hemisphere (Bueš et al., 1974) has been generally accepted. Nevertheless, our findings that the typical CSD-induced changes in DC potential, PO_2, and CBF did not propagate to the contralateral hemisphere serve to strengthen this idea and define the transhemispherical profile more precisely than before (Mayevsky and Weiss, 1991; Back et al., 1994), because all the parameters were continuously and simultaneously recorded and were repeatedly observed in the same animal.

On the other hand, we observed a sustained and bilateral suppression of EEG spectral power in this experiment. Although administration of narcotics alters the peak frequency obtained from power spectral analysis, the frequency domain of EEG signals was relatively constant in anesthetized rats (Chang et al., 1995). The peak frequency obtained in our experiment was limited to the α component range, suggesting that the CSD-induced EEG suppression may be a general neuronal depression rather than an effect on a specific mechanism.

Reduced spontaneous neuronal activity induced by the CSD in the contralateral hemisphere may be related to the phenomenon of diaschisis. Neuronal deactivation in the cerebral cortex by cerebral artery occlusion, topical application of TTX or needle stab-induced CSD reduced blood flow, EEG, and neuronal spontaneous spike rates in the bilateral cerebellar cortex (Gold and Lauritzen, 2002). Furthermore, unilateral application of TTX or CSD reduced cortical spontaneous spike rates in the contralateral sensory cortex (Enager et al., 2004).

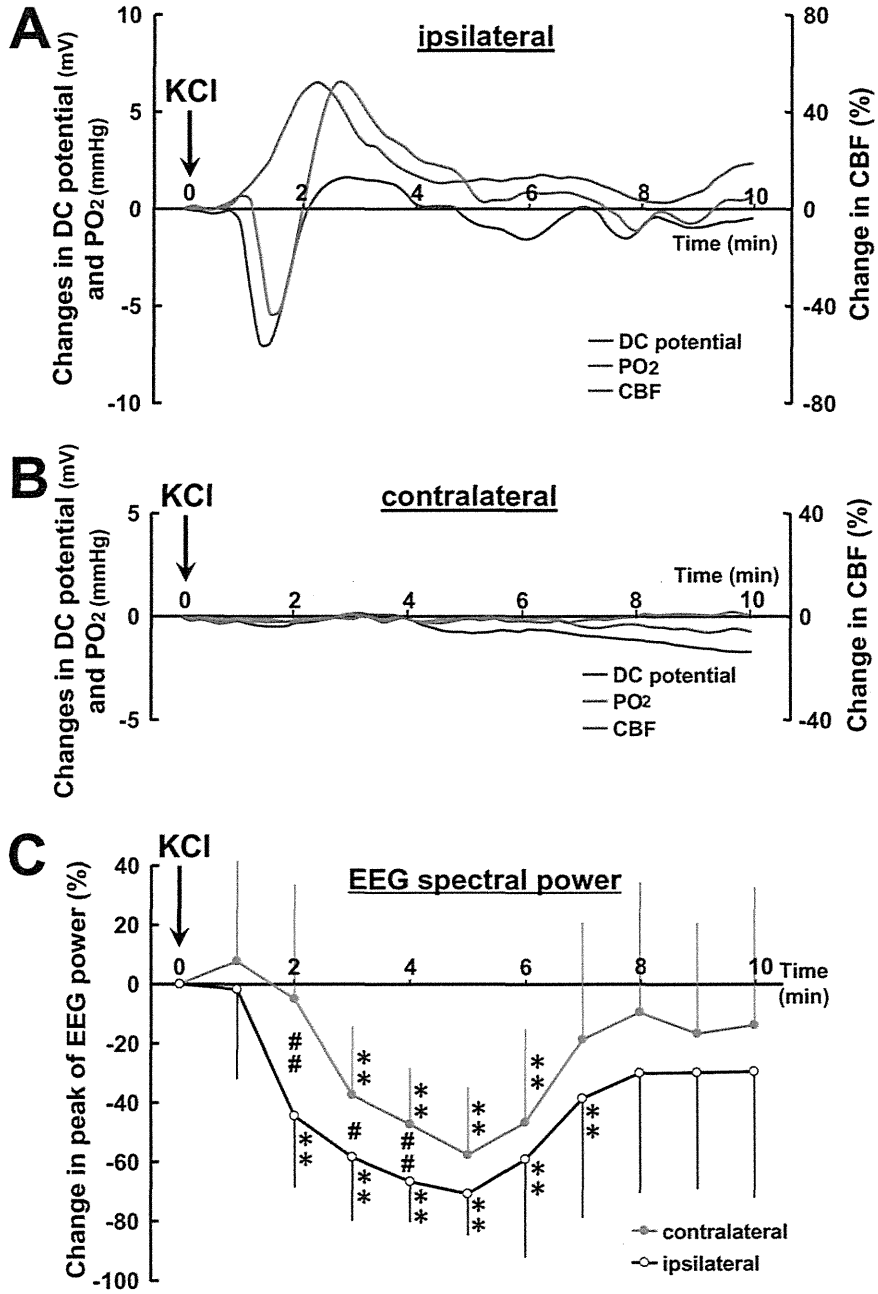

Fig. 3. Average response curves of DC potential, PO_2, CBF, and EEG peak spectral power on the ipsilateral and contralateral sides. Average changes of DC potential (blue), PO_2 (red), and CBF (green) from the level before KCl application for every 10 sec after KCl application are shown for the ipsilateral side (**A**) and the contralateral side (**B**). **C:** Time course of peak EEG spectral power averaged for every 1 min in response to ipsilateral application (open circles) and contralateral application (solid circles) of KCl. $^{**}P < 0.01$ significant difference from the level before KCl application. $^{\#}P < 0.05$, $^{\#\#}P < 0.01$ significant difference between ipsilateral and contralateral sides.

The time course of bilateral suppression of the spike rate was very similar to that of suppression of the EEG spectral power observed in our experiment, so we consider that EEG spectral power reflects the status of spontaneous neuronal activity in the contralateral hemisphere.

Transhemispherical transmission of neuronal activity seems to be mediated via transhemipheric neuronal projections such as corpus callosum (Conti and Manzoni, 1994; Bogdanova and Sil'kis, 1999). This idea is supported by the results showing that electrical stimulation of transcallosal fibers elicited a biphasic postsynaptic potential response, including initial negative potential change (excitation) and following long-lasting positive potential change (inhibition), accompanied by CBF increase (Hoffmeyer et al., 2007). Thus, decrease of excitatory input and/or increase of inhibitory input via

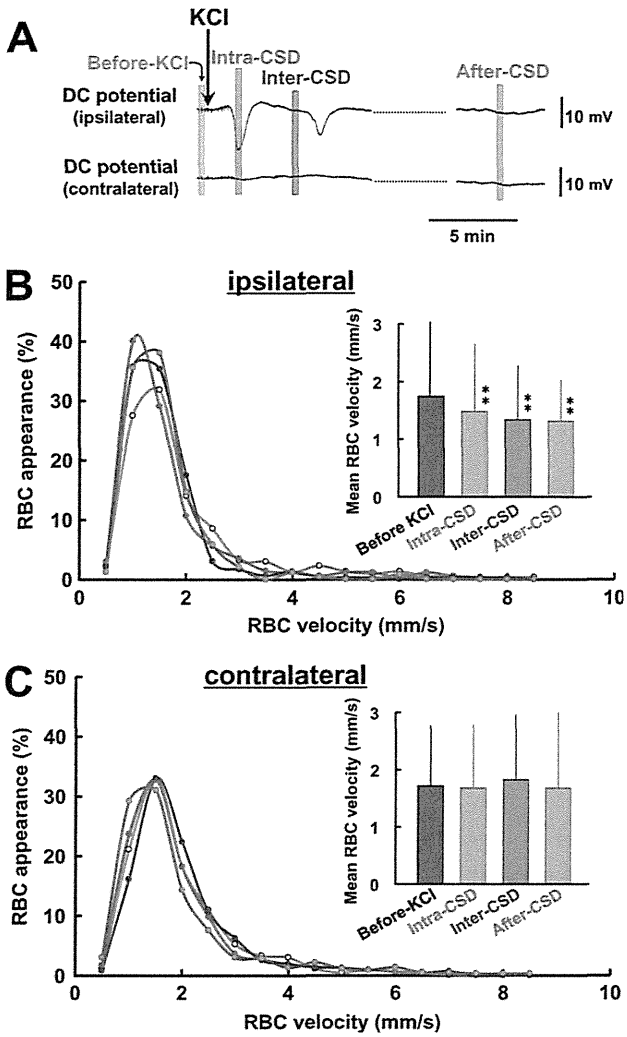

Fig. 4. Summary of RBC velocities in single capillaries. Motion pictures were obtained with the high-speed camera laser scanning confocal microscope at the timings shown in **A**; before KCl application (Before-KCl; gray), just after the trough of DC potential deflection (Intra-CSD; red), several minutes after the DC potential had recovered (Inter-CSD; blue), and 1 hr after KCl application (After-CSD; green). Frequency distribution of RBC velocities in capillaries before and after ipsilateral (**B**) and contralateral (**C**) application of KCl. Average velocities of total detected RBCs are shown in the **insets**. $^{**}P < 0.01$ significant difference from Before-KCl.

interhemispheric projections caused by unilateral CSD might suppress neuronal activity and affect the microcirculation in the contralateral hemisphere.

There have been conflicting reports regarding the response of capillary flow to potassium-induced CSD in the ipsilateral hemisphere, such as an increase of flow concurrently with arterial dilation followed by a relative decrease during oligemia in adult mice (Takano et al., 2007), a fall with an occasional transient cessation in neonatal rats (Chuquet et al., 2007), a transient decrease with occasional full stop in adult rats (Tomita et al., 2005, 2011), and a heterogeneous profile with a long-lasting decrease and a remarkable increase in adult rats (Unekawa et al., 2012). In addition to CSD-induced vasoconstriction following vasodilation of parenchymal arterioles (Osada et al., 2006), neuronal swelling (Takano et al., 2007; Zhou et al., 2010), morphological changes of astrocytes (Tomita et al., 2011), and capillary constriction by oxidative-nitrative stress-induced pericyte contraction (Yemisci et al., 2009) have been described. Thus, capillary resistance might be altered through some physical and/or hemorheological mechanism(s), such as alteration of shear stress and/or hemodilution in nearby capillaries (Hudetz, 1997), increase of plasma viscosity (Tomita et al., 2011), or swelling of endothelial cells, as seen under ischemia/reperfusion (Itoh and Suzuki, 2012). Our present results suggest that sustained neuronal depression alone might be too small to elicit apparent changes in RBC velocity as well as metabolism and local CBF.

CONCLUSIONS

Unilateral application of KCl on the surface of the cerebral cortex induced a short-lasting DC potential deflection with a long-lasting suppression of RBC velocity only in the ipsilateral hemisphere, with neither a typical CSD response nor an RBC velocity change in the contralateral hemisphere. Nevertheless, a significant, long-lasting suppression of EEG spectral power following the CSD events was found in both hemispheres. These findings suggest that CSD-induced changes in RBC velocity in single capillaries might be elicited by mass depolarization of neurons and glial cells in their vicinity, but not by a long-lasting suppression of spontaneous neuronal activity.

ACKNOWLEDGMENTS

The authors declare that they have no conflicts of interest.

REFERENCES

Austin VC, Blamire AM, Grieve SM, O'Neill MJ, Styles P, Matthews PM, Sibson NR. 2003. Differences in the BOLD fMRI response to direct and indirect cortical stimulation in the rat. Magn Reson Med 49:838–847.

Back T, Kohno K, Hossmann KA. 1994. Cortical negative DC deflections following middle cerebral artery occlusion and KCl-induced spreading depression: effect on blood flow, tissue oxygenation, and electroencephalogram. J Cereb Blood Flow Metab 14:12–19.

Bogdanova OG, Sil'kis IG. 1999. The effects of high-frequency microstimulation of the cortex on interhemisphere synchronization in the rat motor cortex. Neurosci Behav Physiol 29:515–522.

Bueš J, Burešová O, Køivánek J. 1974. The mechanism and applications of Leão's spreading depression of electroencephalographic activity. Prague: Academia.

Chang AY, Kuo TB, Tsai TH, Chen CF, Chan SH. 1995. Power spectral analysis of electroencephalographic desynchronization induced by cocaine in rats: correlation with evaluation of noradrenergic neurotransmission at the medial prefrontal cortex. Synapse 21:149–157.

Chuquet J, Hollender L, Nimchinsky EA. 2007. High-resolution in vivo imaging of the neurovascular unit during spreading depression. J Neurosci 27:4036–4044.

Conti F, Manzoni T. 1994. The neurotransmitters and postsynaptic actions of callosally projecting neurons. Behav Brain Res 64:37–53.

del Zoppo GJ. 2010. The neurovascular unit in the setting of stroke. J Intern Med 267:156–171.

Enager P, Gold L, Lauritzen M. 2004. Impaired neurovascular coupling by transhemispheric diaschisis in rat cerebral cortex. J Cereb Blood Flow Metab 24:713–719.

Fabricius M, Lauritzen M. 1993. Transient hyperemia succeeds oligemia in the wake of cortical spreading depression. Brain Res 602:350–353.

Gold L, Lauritzen M. 2002. Neuronal deactivation explains decreased cerebellar blood flow in response to focal cerebral ischemia or suppressed neocortical function. Proc Natl Acad Sci U S A 99:7699–7704.

Hoffmeyer HW, Enager P, Thomsen KJ, Lauritzen MJ. 2007. Nonlinear neurovascular coupling in rat sensory cortex by activation of transcallosal fibers. J Cereb Blood Flow Metab 27:575–587.

Hudetz AG. 1997. Blood flow in the cerebral capillary network: a review emphasizing observations with intravital microscopy. Microcirculation 4:233–252.

Hutchinson EB, Stefanovic B, Koretsky AP, Silva AC. 2006. Spatial flow-volume dissociation of the cerebral microcirculatory response to mild hypercapnia. Neuroimage 32:520–530.

Itoh Y, Suzuki N. 2012. Control of brain capillary blood flow. J Cereb Blood Flow Metab 32:1167–1176.

Kocher M. 1990. Metabolic and hemodynamic activation of postischemic rat brain by cortical spreading depression. J Cereb Blood Flow Metab 10:564–571.

Lauritzen M. 2001. Cortical spreading depression in migraine. Cephalalgia 21:757–760.

Lauritzen M, Jorgensen MB, Diemer NH, Gjedde A, Hansen AJ. 1982. Persistent oligemia of rat cerebral cortex in the wake of spreading depression. Ann Neurol 12:469–474.

Leão A. 1944. Spreading depression of activity in cerebral cortex. J Neurophysiol 7:359–390.

Mayevsky A, Weiss HR. 1991. Cerebral blood flow and oxygen consumption in cortical spreading depression. J Cereb Blood Flow Metab 11:829–836.

Olesen J, Larsen B, Lauritzen M. 1981. Focal hyperemia followed by spreading oligemia and impaired activation of rCBF in classic migraine. Ann Neurol 9:344–352.

Olesen J, Friberg L, Olsen TS, Iversen HK, Lassen NA, Andersen AR, Karle A. 1990. Timing and topography of cerebral blood flow, aura, and headache during migraine attacks. Ann Neurol 28:791–798.

Osada T, Tomita M, Suzuki N. 2006. Spindle-shaped constriction and propagated dilation of arterioles during cortical spreading depression. Neuroreport 17:1365–1368.

Schiszler I, Takeda H, Tomita M, Tomita Y, Osada T, Unekawa M, Tanahashi N, Suzuki N. 2005. Software (KEIO-IS2) for automatically tracking red blood cells (RBCs) with calculation of individual RBC velocities in single capillaries of rat brain. J Cereb Blood Flow Metab 25(Suppl):S541.

Seylaz J, Charbonné R, Nanri K, Von Euw D, Borredon J, Kacem K, Méric P, Pinard E. 1999. Dynamic in vivo measurement of erythrocyte velocity and flow in capillaries and of microvessel diameter in the rat brain by confocal laser microscopy. J Cereb Blood Flow Metab 19:863–870.

Takano T, Tian GF, Peng W, Lou N, Lovatt D, Hansen AJ, Kasischke KA, Nedergaard M. 2007. Cortical spreading depression causes and coincides with tissue hypoxia. Nat Neurosci 10:754–762.

Tomita M, Schiszler I, Tomita Y, Tanahashi N, Takeda H, Osada T, Suzuki N. 2005. Initial oligemia with capillary flow stop followed by hyperemia during K^+-induced cortical spreading depression in rats. J Cereb Blood Flow Metab 25:742–747.

Tomita M, Osada T, Schiszler I, Tomita Y, Unekawa M, Toriumi H, Tanahashi N, Suzuki N. 2008. Automated method for tracking vast numbers of FITC-labeled RBCs in microvessels of rat brain in vivo using a high-speed confocal microscope system. Microcirculation 15:163–174.

Tomita M, Osada T, Unekawa M, Tomita Y, Toriumi H, Suzuki N. 2009. Exogenous nitric oxide increases microflow but decreases RBC attendance in single capillaries in rat cerebral cortex. Microvasc Rev Commun 3:11–16.

Tomita M, Tomita Y, Unekawa M, Toriumi H, Suzuki N. 2011. Oscillating neuro-capillary coupling during cortical spreading depression as observed by tracking of FITC-labeled RBCs in single capillaries. Neuroimage 56:1001–1010.

Unekawa M, Tomita M, Osada T, Tomita Y, Toriumi H, Tatarishvili J, Suzuki N. 2008. Frequency distribution function of red blood cell velocities in single capillaries of the rat cerebral cortex using intravital laser-scanning confocal microscopy with high-speed camera. Asian Biomed 2:203–218.

Unekawa M, Tomita M, Tomita Y, Toriumi H, Suzuki N. 2012. Sustained decrease and remarkable increase of red blood cell velocity in intraparenchymal capillaries associated with potassium-induced cortical spreading depression in rats. Microcirculation 19:166–174.

Williams JL, Shea M, Jones SC. 1993. Evidence that heterogeneity of cerebral blood flow does not involve vascular recruitment. Am J Physiol 264:H1740–H1743.

Yemisci M, Gursoy-Ozdemir Y, Vural A, Can A, Topalkara K, Dalkara T. 2009. Pericyte contraction induced by oxidative-nitrative stress impairs capillary reflow despite successful opening of an occluded cerebral artery. Nat Med 15:1031–1037.

Zhou N, Gordon GR, Feighan D, MacVicar BA. 2010. Transient swelling, acidification, and mitochondrial depolarization occurs in neurons but not astrocytes during spreading depression. Cereb Cortex 20:2614–2624.

3D Analysis of Intracortical Microvasculature during Chronic Hypoxia in Mouse Brains

Kouichi Yoshihara[1], Hiroyuki Takuwa[2], Iwao Kanno[2], Shinpei Okawa[1], Yukio Yamada[1] and Kazuto Masamoto[2,3]

[1]Department of Mechanical Engineering and Intelligent Systems, University of Electro-Communications, Japan, [2]Molecular Imaging Center, National Institute of Radiological Sciences, Japan, [3]Center for Frontier Science and Engineering, University of Electro-Communications, Japan

Abstract The purpose of this study is to determine when and where the brain microvasculature changes its network in response to chronic hypoxia. To identify the hypoxia-induced structural adaptation, we longitudinally imaged cortical microvasculature at the same location within a mouse somatosensory cortex with two-photon microscopy repeatedly for up to one month during continuous exposure to hypoxia (either 8% or 10% oxygen conditions). The two-photon microscopy approach made it possible to track a 3D pathway from a cortical surface arteriole to a venule up to a depth of 0.8 mm from the cortical surface. The network pathway was then divided into individual vessel segments at the branches, and their diameters and lengths were measured. We observed 3 to 11 vessel segments between the penetrating arteriole and the emerging vein over the depths of 20 to 460 μm within the 3D reconstructed image (0.46 x 0.46 x 0.80 mm^3). The average length of the individual capillaries (< 7 μm in diameter) was 67 ± 46 μm, which was not influenced by hypoxia. In contrast, 1.4 ± 0.3 and 1.2 ± 0.2 fold increases of the capillary diameter were observed 1 week after exposure to 8% and 10% hypoxia, respectively. At 3 weeks from the exposure, the capillary diameter reached 8.5 ± 1.9 μm and 6.7 ± 1.8 μm in 8% and 10% hypoxic conditions, respectively, which accounted for the 1.8 ± 0.5 and 1.4 ± 0.3 fold increases relative to those of the prehypoxic condition. The vasodilation of penetrating arterioles (1.4 ± 0.2 and 1.2 ± 0.2 fold increases) and emerging veins (1.3 ± 0.2 and 1.3 ± 0.2 fold increases) showed relatively small diameter changes compared with the parenchymal capillaries. These findings indicate that parenchymal capillaries are the major site responding to the oxygen environment during chronic hypoxia.

1 Introduction

The brain is known to be an organ vulnerable to a lack of oxygen. Only 2 to 3 minutes without an adequate oxygen supply leads to irreversible damage of central

nervous system (CNS) functions. To maintain an adequate supply, the brain vasculature is well organized to allow the diffusion of oxygen to every region of the tissue[1]. Previous studies have shown that the density of brain microvessels adaptively increased in response to chronic hypoxia[2,3]. Angiogenesis and degeneration of the microvasculature were also reported in response to a progress of brain tumors and Alzheimer's disease, respectively[4,5]. These studies strongly indicate that close interaction exists between brain microvasculature and tissue activity to maintain an adequate supply of oxygen. However, the mechanism that regulates the brain microvasculature and its effect on tissue oxygen homeostasis remains mostly unknown.

Because one of the reasons for the lack of knowledge about the structural adaptations of brain microvasculature is a lack of longitudinal studies at the capillary network scale, here, we longitudinally tracked the spatial and temporal adaptation of the microvasculature during chronic hypoxia in a mouse somatosensory cortex with two-photon microscopy. The same three-dimensional (3D) microvasculature was imaged every week for up to one month during continuous exposure to hypoxia (at either 8% or 10% oxygen). Two-photon microscopy is based on the principle of nonlinear optics[6,7,8]. In addition, two-photon microscopy allows excitation with near-infrared light, which has the advantage of providing a long penetration depth in biological tissues[9]. In the present study, volume images of the cortical microvasculature were captured up to a depth of 0.8 mm from the cortical surface with a step size of 0.005 mm and reconstructed with 3D rendering. The 3D pathways of the parenchymal microvasculature were identified and divided into individual segments at the branches. The diameters and lengths of the segments were measured, and their temporal changes were longitudinally traced over the periods of the measurements. Finally, the surface areas and volumes of the vessel segments were calculated to evaluate the adaptation of the microvasculature.

2 Materials and Methods

2.1 Image Analysis

The 3D image (field of view: 0.46×0.46×0.80 mm^3) consists of approximately 160 2D images in the x-y plane parallel to the brain surface with a depth step of 5 μm, and each 2D image has 1024×1024 pixels with an individual pixel size of 0.45 μm. The image analysis performed in each step is described below.

(i) Identification of parenchymal arteriovenous pathway

One target pathway between a surface artery and a vein through parenchymal microvasculature was identified within the reconstructed image (Figs. 1a,b), by

tracking all branches from the artery to the vein including penetrating arterioles, parenchymal capillaries (< 7 μm in diameter), and emerging veins.

(ii) Segmentation of vessels

The vessel segments in the pathway were sequentially numbered (Fig. 1c). One vessel segment was defined as the vessel having two-branches at both ends. The sequential numbers were assigned, beginning from the penetrating artery and ending with the emerging vein.

(iii) Measurement of the length of a vessel segment

The vessel length was measured as the distance from one end to the other end along the centerline of the vessel segment. Several measurement points were manually placed on the centerline to account for the curvature of the vessel. By summing all the distances between the neighboring two measuring points, the vessel length was obtained.

(iv) Measurement of the vessel diameter

The vessel diameter was measured as the average of the diameters at 10 different positions in the vessel segment. Because the intensity differences (i.e., contrast) in the images were sufficient to discriminate the vessel edges relative to the tissue, it was not difficult to manually assign the edges of the vessels to measure the vessel diameters (Fig. 1d).

(v) Calculation of the vessel surface area and volume

The surface areas and volumes of each vessel segment were calculated from the measured diameters and lengths by assuming that each vessel segment was approximated as a cylinder.

2.2. Animal experiments

All experimental protocols were approved by the Institutional Animal Care and Use Committee of the National Institute of Radiological Sciences and the University of Electro-Communications, and the experiments were conducted by following the approved protocols. Ten male C57BL/6J mice (21–23 g) were randomly divided into two groups: one for the 8% oxygen experiment (n=5) and the other for the 10% oxygen experiment (n=5). A custom-made fixation device was fixed to the animal's head for two-photon microscopy imaging[10]. At 2 weeks post-operation, the experiments with hypoxic exposure initiated. During the imaging experiments, the mice were anesthetized with isoflurane (1%) in a mixture of air and oxygen gas, and their rectal temperature was maintained at 37±1°C. Sulforhodamine 101 (SR101) dissolved in saline (5 mM) was intraperitoneally injected into the animal (8 mL/kg) for labeling blood plasma, and cortical vasculature was imaged with a two-photon microscope (TCS SP5MP, Leica Microsystems, Germany) equipped with a Ti:Sapphire laser (MaiTai HP, Spectra-Physics, CA). The excitation wavelength was 900 nm (average power 2.0 W output), and the emission signal was detected through a bandpass filter (610/75 nm).

At day 0 (start of exposure to hypoxia), a reference image of the cortical surface vasculature was obtained with reflection acquisition mode excited at 633 nm with a low magnification object lens (field of view: 3.6×3.6 mm^2). The cortical arteries and veins were distinguished in the reflection image; the arteries and veins exhibited different light intensities because of their different light absorption characteristics[9]. Because the pattern of the cortical surface vessels was preserved over the period of the longitudinal experiments, the reference image was used to identify the measurement locations at different imaging experiments. Except while undergoing imaging, the animals were kept in either an 8% or 10% oxygen room in which the oxygen level was monitored with an oxygen sensor. The imaging experiments were repeatedly performed on days 0, 7, 14, 21, and 31 after exposure to hypoxia. Because 3 out of 5 animals were dead after 3 weeks in the 8% oxygen experiment, the analytical results were only compared for the first 3 weeks of measurements. Data were represented as mean ± standard deviation.

3. Results and Discussion

Reconstructed 3D images of cortical microvasculature are represented in Fig. 2. The images show the apparently same 3D structures over the period of one month during continuous exposure to hypoxia. The 3D pathways were identified from penetrating arteriole (A) to emerging vein (V) through parenchymal capillaries (C), which had 5 to 13 branches between the surface artery and the vein over depths of 20 to 460 μm within the image. The total length from the beginning of a penetrating arteriole to the end point of the emerging vein was 703 ± 278 μm (311 -1221 μm, n=30 networks), which was unchanged during chronic hypoxia over 3 weeks (Table 1). In contrast, the parenchymal capillary diameter was predominantly increased by 1.4 ± 0.3 and 1.2 ± 0.2 fold at 1 week after continuous exposure to 8% and 10% oxygen, respectively (Table 1). The vasodilation of parenchymal capillaries continued over 3 weeks: 1.8 ± 0.5 and 1.4 ± 0.3 fold relative to that of the prehypoxic condition. This increase was significantly higher than both the penetrating arterioles (1.4 ± 0.2 times) and emerging veins (1.3 ± 0.2 times) under the 8% oxygen condition but not the 10% oxygen condition (1.2 ± 0.2 fold for arterioles and 1.3 ± 0.2 fold for veins). Consequently, the vessel surface area increased by 1.5 ± 0.4, 1.8 ± 0.7, and 1.2 ± 0.3 fold for arterioles, capillaries, and veins after 3 weeks under 8% oxygen exposure and by 1.2 ± 0.3, 1.4 ± 0.5, and 1.3 ± 0.3 fold for 10% oxygen, respectively. In addition, the vessel volume was 2.1 ± 0.9, 3.5 ± 2.5, and 1.7 ± 0.6 times larger for 8% oxygen and 1.6 ± 0.5, 2.1 ± 1.6, and 1.6 ± 0.6 times larger for 10% oxygen. These results show that depending on the level of hypoxia, vascular restructuring was induced for different vessel types. In particular, the lower oxygen level (8%) caused a predominant increase in the parenchymal capillary volumes, indicating that several mechanisms may be participating in the hypoxia-induced restructuring of cortical microvasculature. Future studies are needed to investigate the mechanism

of oxygen level sensing and the driving force leading to a change in the capillary diameter to further understand the mechanism involved in maintaining tissue oxygen homeostasis in the brain.

4. Conclusions

The present study quantified hypoxia-induced restructuring of cerebral microvasculature based on 3D network pathways measured with two-photon microscopy at the same locations within mouse brains over one month. We found that hypoxia-induced vasodilation occurred predominantly in the parenchymal capillaries, indicating that parenchymal capillaries are the major site responding to the chronic hypoxic environment.

Acknowledgments The authors thank Mr. Ryutaro Asaga and Mr. Ryota Sakamoto for their help in the preparation of the experiments. This work was partially supported by Special Coordination Funds for Promoting Science and Technology (K.M.).

References

1. Masamoto K, Tanishita K (2009) Oxygen transport in brain tissue. J Biomech Eng 131: 074002
2. Boero JA, Ascher J, Arregui A et al (1999) Increased brain capillaries in chronic hypoxia. J Appl Physiol 86:1211-1219
3. Xu K, LaManna JC (2006) Chronic hypoxia and the cerebral circulation. J Appl Physiol 100:725-730
4. Wsseling P, Ruiter DJ, Burger PC (1997) Angiogenesis in brain tumors; pathobiological and clinical aspects. J Neurooncol 32:253-265
5. Meyer EP, Ulmann-Schuler A, Staufenbiel M et al (2008) Altered morphology and 3D architecture of brain vasculature in a mouse mode for Alzheimer's disease. Proc Natl Acad Sci U S A 105:3587-3592
6. Denk W, Strickler JH, Webb WW (1990) Two-photon laser scanning fluorescence microscopy. Science 248:73-76
7. So PT, Dong CY, Masters BR et al (2000) Two-photon excitation fluorescence microscopy. Annu Rev Biomed Eng 2:399-429
8. Helmchen F, Denk W (2005) Deep tissue two-photon microscopy. Nat Methods 2:932-940
9. Yamada Y (1995) Light-tissue interaction and optical imaging in biomedicine. Annual Review of Heat Transfer (Begell house, Inc.) 6:1-59
10. Takuwa H, Autio J, Nakayama H et al (2011) Reproducibility and variance of a stimulation-induced hemodynamic response in barrel cortex of awake behaving mice. Brain Res 1369: 103-111

Table 1 Vessel diameter and length measurements of single pathways from a penetrating arteriole (A) to the emerging vein (V) through parenchymal capillaries (C, < 7 μm in diameter) during chronic hypoxia

i) 8% O_2 (n=5)

	Diameter (μm)				Length (μm)			
(total #)	day 0	day 7	day 14	day 21	day 0	day 7	day 14	day 21
A (32)	11±5	14±5	15±5	16±6	77±41	78±39	76±41	77±38
C (61)	4.9±0.9	6.8±1.3	7.5±1.7	8.5±1.9	68±48	69±49	67±46	67±46
V (23)	17±9	21±10	23±12	23±13	91±69	88±66	86±61	81±58

ii) 10% O_2 (n=5)

	Diameter (μm)				Length (μm)			
(total #)	day 0	day 7	day 14	day 21	day 0	day 7	day 14	day 21
A (42)	14±6	17±7	18±7	18±7	126±108	123±108	122±106	123±106
C (69)	5.0±1.0	5.9±1.4	6.4±1.5	6.7±1.8	61±37	62±36	60±36	61±35
V (21)	17±8	19±8	20±9	21±10	136±127	141±122	134±121	133±119

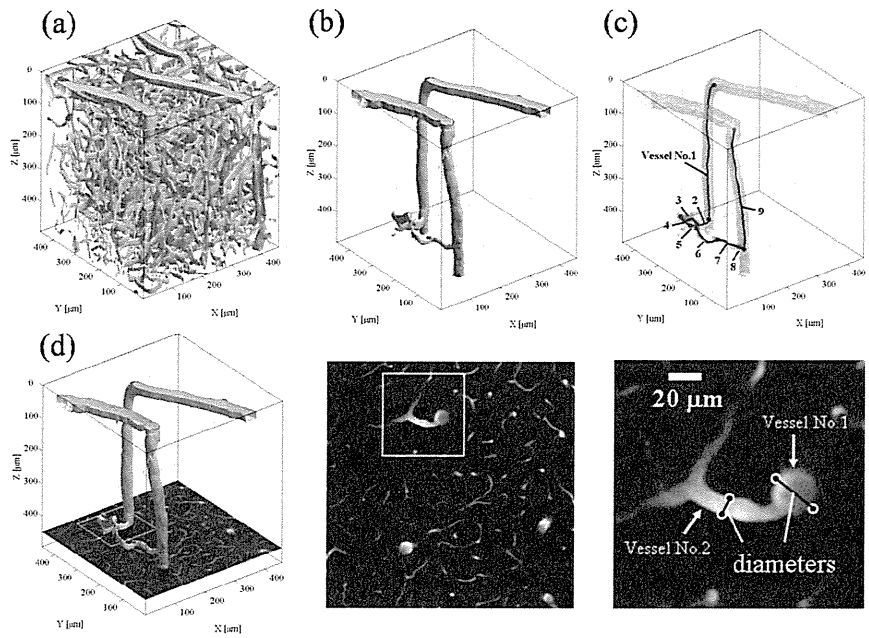

Figure 1. Methods for measuring vessel diameter and length. (a) Reconstructed volume image of parenchymal microvasculature; binarized from 3D image that was reconstructed by rendering obtained 2D x-y images. (b) Selection of a single vessel pathway; the selection criterion was to have the entire connection from the surface arteriole to the surface venule visible within the image. (c) Segmentation and measurement of the length of individual vessel segments. (d) Manual measurement of vessel diameter in the image.

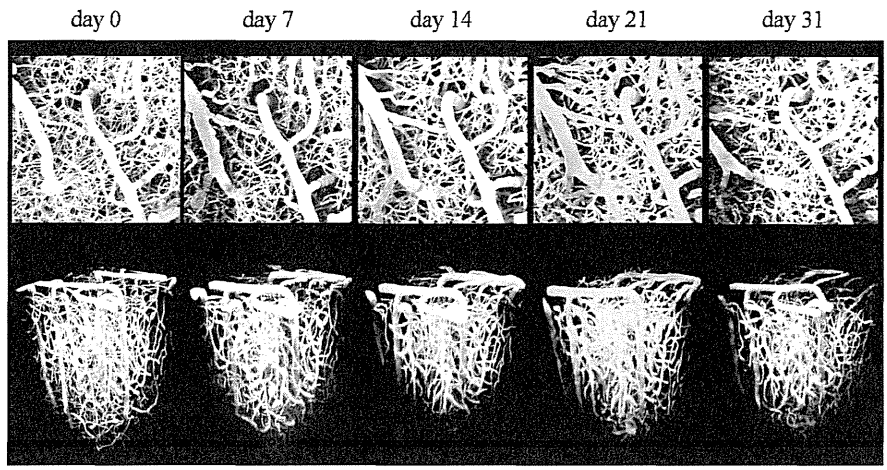

Figure 2. The 3D imaging of cortical microvasculature with two-photon microscopy. Volume images ($0.46\times0.46\times0.80$ mm^3) were obtained from day 0 (start of exposure to 10% oxygen) to day 31 for the identical region within the cortex. The upper panels show the maximum intensity projected images in the x-y plane (0.46×0.46 mm^2), and the lower panels show the 3D reconstructed images.

Chapter 23
Dynamic Two-Photon Imaging of Cerebral Microcirculation Using Fluorescently Labeled Red Blood Cells and Plasma

Kazuto Masamoto, Hiroshi Kawaguchi, Hiroshi Ito, and Iwao Kanno

Abstract To explore the spatiotemporal dynamics of red blood cells (RBCs) and plasma flow in three-dimensional (3D) microvascular networks of the cerebral cortex, we performed two-photon microscopic imaging of the cortical microvasculature in genetically engineered rats in which the RBCs endogenously express green fluorescent protein (GFP). Water-soluble quantum dots (Qdots) were injected intravenously into the animals to label the plasma, and concurrent imaging was performed for GFP-RBCs and Qdot plasma. The RBC and plasma distributions were compared between resting state and forepaw stimulation-induced neural activation. The RBC and plasma images showed detectable signals up to a depth of 0.4 and 0.6 mm from the cortical surface, respectively. A thicker plasma layer (2–5 μm) was seen in venous vessels relative to the arterial vessels. In response to neural activation, the RBCs were redistributed among the parenchymal capillary networks. In addition, individual capillaries showed a variable ratio of RBC and plasma distributions before and after activation, indicative of dynamic changes of hematocrit in single capillaries. These results demonstrate that this transgenic animal model may be useful in further investigating the mechanism that controls dynamic RBC flow in single capillaries and among multiple capillary networks of the cerebral microcirculation.

Keywords Brain microcirculation • Functional imaging • Oxygen demand and supply • Somatosensory cortex

K. Masamoto, Ph.D. (✉)
Center for Frontier Science and Engineering, University of Electro-Communications, 1-5-1 Chofugaoka, Chofu, Tokyo 182-8585, Japan

Molecular Imaging Center, National Institute of Radiological Sciences, Chiba, Japan
e-mail: masamoto@mce.uec.ac.jp

H. Kawaguchi • H. Ito • I. Kanno
Molecular Imaging Center, National Institute of Radiological Sciences, Chiba, Japan

W.J. Welch et al. (eds.), *Oxygen Transport to Tissue XXXIV*, Advances in Experimental Medicine and Biology 765, DOI 10.1007/978-1-4614-4989-8_23,

1 Introduction

Two-photon microscopy allows for three-dimensional (3D) microscopic imaging of animal brains in vivo with deep penetration of near-infrared excitation light [1, 2]. In previous studies, we have shown that 3D images of cortical microvasculature can be obtained up to a depth of 0.6 mm in rats with thinned skulls [3] and 0.8 mm in mice with a closed cranial window [4]. However, these studies are limited to only structural imaging and are not investigated for measuring blood flow, which is of particular importance for understanding oxygen transport to tissues in living brains.

With two-photon microscopy, Kleinfeld et al. introduced a line-scanning method for measuring red blood cell (RBC) speed in single capillaries [5]. Later studies have successfully employed a variety of methods for the quantification of capillary RBC speed [6–11]. With a high-speed frame rate (500 frames/s), Tomita et al. created a 2D RBC speed map in rat and mouse cerebral cortex [12–14]. In their studies, fluorescently labeled RBCs were injected to create contrast within the circulation, which allows for the tracking of individual RBCs in multiple vessels simultaneously using a confocal laser-scanning microscope. However, the labeled RBCs represent only a portion of the RBCs resident in the circulation, and thus, vessel occupancy of the RBCs relative to plasma levels, i.e., hematocrit, cannot be resolved using this technique.

In the present study, we performed dynamic two-photon imaging of cortical microvasculature using genetically engineered rats in which whole RBCs were endogenously labeled with green fluorescent protein (GFP). In addition, we injected the animals with water-soluble quantum dots (Qdots) that act as a plasma marker [15]. The selected Qdots had a peak emission in the red spectrum at a wavelength of 605 nm, which allowed for simultaneous imaging of GFP-RBCs and Qdot plasma. We compared RBC and plasma distributions in single capillaries and among multiple capillaries under the conditions of rest and forepaw stimulation-induced activation in the somatosensory cortex.

2 Materials and Methods

2.1 Animal Preparation

All experimental protocols were approved by the Institutional Animal Care and Use Committee. A total of eight male transgenic Wistar rats (250–480 g) were used for the experiments. The animals were anesthetized with 2% isoflurane for surgery and 1.4% for experiments. Intubation was performed for mechanical ventilation. The femoral artery was catheterized with a PE50 tube for monitoring the arterial blood pressure and blood gas sampling, and the femoral vein was catheterized with a PE10 tube for drug administration. The rectal temperature was maintained at 37°C. The animal was fixed on a stereotactic frame, and the left somatosensory cortex was exposed by removing the skull with a dental drill, leaving a layer of thinned dura. The exposed area was covered with warm saline (37°C), and the experiments were